Geophys. J. Int. (2004) **156,** 171–178 doi: 10.1111/j.1365-246X.2003.02150.x

Love's problem

Janet M. Becker[1] and Michael Bevis[2]

[1]*Department of Geology and Geophysics, University of Hawaii,* 1680 *East–West Road, Post* 813, *Honolulu, Hawaii,* 96822, *USA. E-mail: jbecker@soest.hawaii.edu*

[2]*Hawaii Institute of Geophysics and Planetology University of Hawaii at Manoa, Honolulu, Hawaii,* 96822, *USA*

Accepted 2003 September 2. Received 2003 July 23; in original form 2002 November 4

SUMMARY

Explicit expressions for the displacements generated in a non-gravitating, homogeneous, semi-infinite half-space by uniform surface pressure applied over a rectangular region are presented. These complement expressions for the associated stress field given by Love in 1929.

Key words: crustal deformation, flexure of the lithosphere, lithospheric deformation, numerical techniques.

1 INTRODUCTION

The problem of the surface loading of a Cartesian elastic half-space is associated with the name of Boussinesq (1885) who showed that the components of displacement and stress at any point within the half-space can be expressed in terms of the various spatial derivatives of elastic potential functions. Many people have contributed to this area of elasticity theory by producing explicit expressions for the deformations produced in response to a surface pressure distribution of specific shape and form. For example, Boussinesq (1885) provided the solution for a point load, while Lamb (1902) and Terazawa (1916), using Fourier–Bessel transforms, addressed the case of uniform pressure applied within a circular boundary. Love (1929) revisited the problem of the circular or disc load using Boussinesq's potential method. He also introduced a new class of loading problem—that of uniform pressure applied within a rectangular region of the surface. We refer to this as Love's problem. Love (1929) presented only a partial solution to this problem, in that he provided expressions for the stress field within the half-space, but not for the displacement field. Presumably this omission reflects the technical motivation of his study—that of the safety of foundations.

In many cases of practical interest, the surface load is not laterally uniform. Multiple disc loads often are used to approximate laterally varying surface loads; however, a flat surface is much easier to tile with rectangles. By solving Love's problem, we provide a convenient basis for modelling arbitrary surface loads applied to an elastic half-space.

Crustal motion geodesists have become increasingly interested in elastic loading signals manifest as seasonal fluctuations in the position time-series produced at continuous GPS stations and by related space geodetic techniques (Heki 2001; Mangiarotti *et al.* 2001; Dong *et al.* 2002; Elósegui *et al.* 2003). These surface loads are associated with changes in atmospheric and seafloor pressure, and shifting masses of snow, ice, and surface and subsurface water. Many problems associated with localized loads have a spatial scale which is very small compared with the radius of the Earth, allowing the problem to be analysed within the framework of a Cartesian half-space. In most parts of the world if these loads are applied for time periods of $\sim$1 yr of less, then viscous effects may be neglected and we may assume an elastic structure for the half-space. In some cases it may be appropriate to assume a uniform elastic half-space, at least as a first approximation. Of course, well established numerical techniques exist for analysing loading problems with more complex Earth models that incorporate the Earth's curvature and radial variation in elastic structure (Farrell 1972; Elósegui *et al.* 2003). Nevertheless, the solution to Love's problem may be of interest because it may provide a reasonable approximation in some contexts, or because it may be used to test computer codes based on more sophisticated geoelastic models.

2 PROBLEM STATEMENT

We consider here the displacements generated by a uniform pressure, p, applied over a rectangular region described by $-a \leq x \leq a$, $-b \leq y \leq b$ at the surface ($z = 0$) of a semi-infinite solid (Fig. 1) where z is positive downward so that points in the solid have $z > 0$. Following Love (1929), we take x, y, z to be the coordinates of a point within the solid and $x', y', 0$ to be those of a point on the plane boundary and denote the distance between these points by r where

$$r^2 = \Delta x^2 + \Delta y^2 + z^2, \tag{1}$$

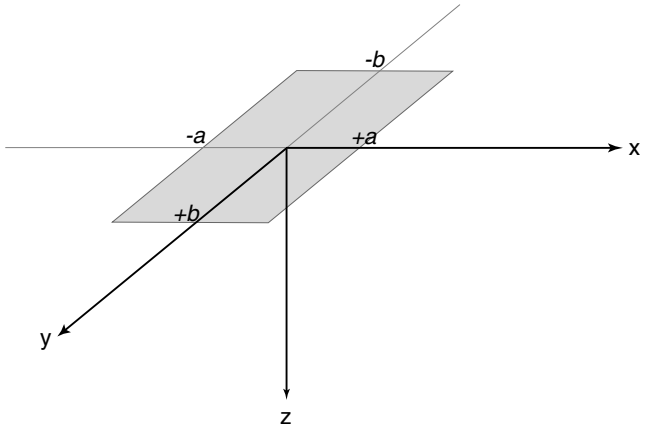

Figure 1. Rectangular region of uniform applied pressure at the surface of a semi-infinite ($z \geq 0$) elastic solid.

$\Delta x = x' - x$, $\Delta y = y' - y$ and $r > 0$. The displacements u, v, w generated by this applied pressure are given by

$$\begin{aligned} u &= -\frac{1}{4\pi}\left(\frac{1}{\lambda+\mu}\frac{\partial \chi}{\partial x} + \frac{z}{\mu}\frac{\partial V}{\partial x}\right) \\ v &= -\frac{1}{4\pi}\left(\frac{1}{\lambda+\mu}\frac{\partial \chi}{\partial y} + \frac{z}{\mu}\frac{\partial V}{\partial y}\right) \\ w &= \frac{1}{4\pi\mu}\left(\frac{\lambda+2\mu}{\lambda+\mu}V - z\frac{\partial V}{\partial z}\right), \end{aligned} \tag{2}$$

where λ and μ are the Lame constants,

$$\chi = \int_{-a}^{a}\int_{-b}^{b} p \log(z+r)\, dx'\, dy' \tag{3}$$

is Boussinesq's 3-D logarithmic potential, and

$$V = \int_{-a}^{a}\int_{-b}^{b} p r^{-1}\, dx'\, dy' \tag{4}$$

is the Newtonian potential of a surface distribution. We note that for a uniform pressure, p, χ and V depend upon Δx and Δy so that, for example, $-\frac{\partial \chi}{\partial x} = \frac{\partial \chi}{\partial x'}$, which will prove useful in what follows. We derive here analytic expressions for the displacements in forms that are straightforward to implement numerically.

2.1 Horizontal displacements

Following Love (1929), we define

$$\begin{aligned} r_{j0}^2 &= r^2|_{x'=\pm a} = (a \mp x)^2 + \Delta y^2 + z^2, \qquad r_{j0} > 0 \\ \beta_{j0}^2 &= r_{j0}^2 - \Delta y^2 = (a \mp x)^2 + z^2, \qquad \beta_{j0} > 0 \end{aligned} \tag{5}$$

and introduce

$$\psi_{j0} = \frac{\Delta y}{r_{j0} + \beta_{j0}}, \qquad \psi_{j0}^2 < 1 \quad (j = 1, 2),$$

where hereinafter the upper(lower) signs correspond to $j = 1(2)$.

To obtain an explicit expression for the u-displacement, we take $-\frac{1}{p}\frac{\partial}{\partial x}$ of (3) to obtain

$$-\frac{1}{p}\frac{\partial \chi}{\partial x} = \int_{-b}^{b}\int_{-a}^{a} \frac{\partial}{\partial x'}\left[\log(z+r)\right] dx' dy' = (J_1 - J_2)_{y'=-b}^{y'=b}, \tag{6}$$

where

$$J_j = \int \log(z + r_{j0})\, dy' \quad (j = 1, 2). \tag{7}$$

Similarly,

$$-\frac{1}{p}\frac{\partial V}{\partial x} = \int_{-b}^{b}\int_{-a}^{a} \frac{\partial}{\partial x'}\left(\frac{1}{r}\right) dx' dy' = (\mathcal{J}_1 - \mathcal{J}_2)_{y'=-b}^{y'=b}, \tag{8}$$

where

$$\mathcal{J}_j = \int \frac{1}{r_{j0}} dy' \quad (j = 1, 2). \tag{9}$$

To evaluate (7) and (9), we change variables following Love (1929) according to

$$\begin{aligned} \Delta y &= \beta_{j0}\tan\theta, \qquad dy' = \beta_{j0}\sec^2\theta\, d\theta \\ r_{j0} &= \beta_{j0}\sec\theta, \end{aligned} \tag{10}$$

where $-\frac{\pi}{2} < \theta < \frac{\pi}{2}$ so that r_{j0} remains positive. Substituting (10) into (7), we obtain

$$J_j = \int \log(z+\beta_{j0}\sec\theta)\beta_{j0}\sec^2\theta\, d\theta. \tag{11}$$

Integrating by parts yields

$$J_j = \beta_{j0}\left[\log(z+\beta_{j0}\sec\theta)\tan\theta - \beta_{j0}\int \frac{\sec\theta\tan^2\theta}{z+\beta_{j0}}\, d\theta\right]. \tag{12}$$

We evaluate the integral in (12) using Mathematica to obtain

$$\begin{aligned} \beta_{j0}\int \frac{\sec\theta\tan^2\theta}{z+\beta_{j0}\sec\theta}d\theta &= \tan\theta + \frac{2}{\beta_{j0}}\sqrt{z-\beta_{j0}}\sqrt{z+\beta_{j0}}\tanh^{-1}\left(\frac{\sqrt{z-\beta_{j0}}}{\sqrt{z+\beta_{j0}}}\tan\frac{\theta}{2}\right) \\ &\quad + \frac{z}{\beta_{j0}}\log\left(\frac{\cos\frac{\theta}{2}-\sin\frac{\theta}{2}}{\cos\frac{\theta}{2}+\sin\frac{\theta}{2}}\right). \end{aligned} \tag{13}$$

We note that it is straightforward to verify (13) by differentiation. Transforming (12) back to our original variables, we obtain after some algebra

$$J_j = \Delta y\left[\log(z+r_{j0})-1\right] + z\log\left(\frac{1+\psi_{j0}}{1-\psi_{j0}}\right) + 2|a\mp x|\tan^{-1}\left(\frac{|a\mp x|\psi_{j0}}{z+\beta_{j0}}\right). \tag{14}$$

To evaluate (9), we again change variables according to (10) to obtain

$$\begin{aligned} \mathcal{J}_j &= \int \frac{1}{r_{j0}}dy' = \int \sec\theta\, d\theta \\ &= \log(\sec\theta+\tan\theta) = \log\left(\tfrac{\Delta y + r_{j0}}{\beta_{j0}}\right). \end{aligned} \tag{15}$$

We note that

$$\left[\mathcal{J}_j\right]_{y'=-b}^{y'=b} = \left[\log(\Delta y + r_{j0})\right]_{y'=-b}^{y'=b} \tag{16}$$

since β_{j0} is independent of Δy.

The calculation for the v-displacement proceeds similarly with

$$\begin{aligned} r_{0j}^2 &= r^2|_{y'=\pm b} = \Delta x^2 + (b\mp y)^2 + z^2, \qquad r_{0j} > 0 \\ \beta_{0j}^2 &= r_{0j}^2 - \Delta x^2 = (b\mp y)^2 + z^2, \qquad \beta_{0j} > 0 \end{aligned} \tag{17}$$

and

$$\psi_{0j} = \frac{\Delta x}{r_{0j}+\beta_{0j}}, \qquad \psi_{0j}^2 < 1 \quad (j=1,2)$$

The required integrals include

$$-\frac{1}{p}\frac{\partial\chi}{\partial y} = \int_{-a}^{a}\int_{-b}^{b}\frac{\partial}{\partial y'}\left[\log(z+r)\right]dy'dx' = (K_1-K_2)_{x'=-a}^{x'=a}, \tag{18}$$

where

$$K_j = \int \log(z+r_{0j})\, dx' \quad (j=1,2) \tag{19}$$

and

$$-\frac{1}{p}\frac{\partial V}{\partial y} = \int_{-a}^{a}\int_{-b}^{b}\frac{\partial}{\partial y'}\left(\frac{1}{r}\right)dy'dx' = (\mathcal{K}_1-\mathcal{K}_2)_{x'=-a}^{x'=a}, \tag{20}$$

where

$$\mathcal{K}_j = \int \frac{1}{r_{0j}}dx' \quad (j=1,2). \tag{21}$$

As with the u-displacement, we change variables according to

$$\begin{aligned} \Delta x &= \beta_{0j}\tan\theta, \qquad dx' = \beta_{0j}\sec^2\theta\, d\theta \\ r_{0j} &= \beta_{0j}\sec\theta, \end{aligned} \tag{22}$$

where $-\frac{\pi}{2} < \theta < \frac{\pi}{2}$ so that r_{0j} remains positive and obtain

$$K_j = \Delta x\left[\log(z+r_{0j})-1\right] + z\log\left(\frac{1+\psi_{0j}}{1-\psi_{0j}}\right) + 2|b\mp y|\tan^{-1}\left(\frac{|b\mp y|\psi_{0j}}{z+\beta_{0j}}\right). \tag{23}$$

Also,

$$\mathcal{K}_j = \int \frac{1}{r_{0j}} dx' = \int \sec\theta d\theta$$
$$= \log(\sec\theta + \tan\theta) = \log\left(\frac{\Delta x + r_{0j}}{\beta_{0j}}\right) \tag{24}$$

and

$$\left[\mathcal{K}_j\right]_{x'=-a}^{x'=a} = \left[\log(\Delta x + r_{0j})\right]_{x'=-a}^{x'=a} \tag{25}$$

since β_{0j} is independent of Δx.

2.2 Vertical displacement

To obtain an analytic expression for the vertical displacement w, we require both V and $\frac{\partial V}{\partial z}$. We begin by deriving an expression for $\frac{\partial V}{\partial z}$. Taking $-\frac{1}{p}\frac{\partial}{\partial z}$ of (4), we obtain

$$-\frac{1}{p}\frac{\partial V}{\partial z} = \int_{-b}^{b}\int_{-a}^{a} \frac{z}{r^3} dx' dy'. \tag{26}$$

Following our derivation of the horizontal displacements, we rewrite the integrand in (26) as

$$\frac{z}{r^3} = \frac{\partial}{\partial x'}\left[\frac{z\Delta x}{(\Delta y^2 + z^2)r} + f(\Delta y, z)\right], \tag{27}$$

where f is an arbitrary function. Then (26) becomes

$$-\frac{1}{p}\frac{\partial V}{\partial z} = \int_{-b}^{b}\left[\frac{z\Delta x}{(\Delta y^2 + z^2)r} + f(\Delta y, z)\right]_{x'=-a}^{x'=a} dy' = (P_1 + P_2)_{y'=-b}^{y'=b}, \tag{28}$$

where

$$P_j = z(a \mp x)\int \frac{dy'}{(\Delta y^2 + z^2)r_{j0}} \tag{29}$$

since f is independent of Δx. To evaluate the integral in (29), we transform variables according to (10) to obtain

$$P_j = z(a \mp x)\int \frac{\sec\theta d\theta}{\beta_{j0}^2 \tan^2\theta + z^2} = z(a \mp x)\int \frac{d\xi}{(a \mp x)\xi^2 + z^2}, \tag{30}$$

where $\xi = \sin\ \theta$; hence,

$$P_j = \tan^{-1}\frac{(a \mp x)\Delta y}{z r_{j0}}. \tag{31}$$

Equivalently, we may rewrite the integrand in (26) as

$$\frac{z}{r^3} = \frac{\partial}{\partial y'}\left[\frac{z\Delta y}{(\Delta x^2 + z^2)r} + g(\Delta x, z)\right], \tag{32}$$

where g is an arbitrary function. Proceeding as in (26)–(30), but using the variable transformation (22), we obtain

$$-\frac{1}{p}\frac{\partial V}{\partial z} = (Q_1 + Q_2)_{x'=-a}^{x'=a}, \tag{33}$$

where

$$Q_j = \tan^{-1}\frac{(b \mp y)\Delta x}{z r_{0j}}. \tag{34}$$

We note that it is straightforward to show that (28) and (33) are equivalent.

We proceed similarly to obtain two expressions for the Newtonian potential, V, given in (4) and repeated here for convenience

$$\frac{1}{p}V = \int_{-b}^{b}\int_{-a}^{a} \frac{1}{r} dx' dy'. \tag{35}$$

The integrand in (35) may be expressed as

$$\frac{1}{r} = \frac{\partial[\log(\Delta x + r) + f(\Delta y, z)]}{\partial x'}, \tag{36}$$

where f is an arbitrary function. Then,

$$\frac{1}{p}V = \int_{-b}^{b}\{[\log(\Delta x + r) + f(\Delta y, z)]\}_{-a}^{a}\, dy' = (L_1 - L_2)_{y'=-b}^{y'=b}, \tag{37}$$

where

$$L_j = \int \log(\pm a - x + r_{j0})\, dy'. \tag{38}$$

The integral in (38) is isomorphic to (7) and may be evaluated accordingly to obtain

$$L_j = \Delta y \left[\log(\pm a - x + r_{j0}) - 1\right] + (\pm a - x)\log\left(\frac{1+\psi_{j0}}{1-\psi_{j0}}\right) + 2z\tan^{-1}\left[\frac{z\psi_{j0}}{(\pm a - x) + \beta_{j0}}\right]. \tag{39}$$

Equivalently, we may rewrite the integrand in (35) as

$$\frac{1}{r} = \frac{\partial[\log(\Delta y + r) + g(\Delta x, z)]}{\partial y'}. \tag{40}$$

Then, it is straightforward to show that

$$\frac{1}{p}V = (M_1 - M_2)_{x'=-a}^{x'=a}, \tag{41}$$

where

$$M_j = \Delta x \left[\log(\pm b - y + r_{0j}) - 1\right] + (\pm b - y)\log\left(\frac{1+\psi_{0j}}{1-\psi_{0j}}\right) + 2z\tan^{-1}\left[\frac{z\psi_{0j}}{(\pm b - y) + \beta_{0j}}\right]. \tag{42}$$

3 SUMMARY

We summarize our results for the horizontal displacements

$$u = -\frac{p}{4\pi}\left[\frac{1}{\lambda+\mu}(J_2 - J_1) + \frac{z}{\mu}\log\left(\frac{\Delta y + r_{20}}{\Delta y + r_{10}}\right)\right]_{y'=-b}^{y'=b} \tag{43}$$

$$v = -\frac{p}{4\pi}\left[\frac{1}{\lambda+\mu}(K_2 - K_1) + \frac{z}{\mu}\log\left(\frac{\Delta x + r_{02}}{\Delta x + r_{01}}\right)\right]_{x'=-a}^{x'=a}, \tag{44}$$

where J_j and K_j are given by (14) and (23), respectively.

For the vertical displacements

$$w = \frac{p}{4\pi\mu}\left[\frac{\lambda+2\mu}{\lambda+\mu}(L_1 - L_2) + z\left\{\tan^{-1}\frac{(a-x)\Delta y}{z r_{10}} + \tan^{-1}\frac{(a+x)\Delta y}{z r_{20}}\right\}\right]_{y'=-b}^{y'=b} \tag{45}$$

or

$$w = \frac{p}{4\pi\mu}\left\{\frac{\lambda+2\mu}{\lambda+\mu}(M_1 - M_2) + z\left[\tan^{-1}\frac{(b-y)\Delta x}{z r_{01}} + \tan^{-1}\frac{(b+y)\Delta x}{z r_{02}}\right\}\right]_{x'=-a}^{x'=a},$$

where L_j and M_j are given by (39) and (42), respectively.

4 NUMERICAL VERIFICATION

4.1 An idealized lake load: surface displacements

We consider the elastic surface displacements generated by an applied pressure equivalent to 100 m water depth in a rectangular area 2 × 1 km^2 (Fig. 2a). We assume that Young's modulus $E = \frac{\mu(3\lambda+2\mu)}{\lambda+\mu} = 0.6 \times 10^{11}$ Nm^{-2} and Poisson's ratio $\nu = \frac{\lambda}{2(\lambda+\mu)} = 0.25$. We set the surface pressure $p = \rho gh$ where $\rho = 1000$ kg m^{-3}, $h = 100$ m, and $g = 9.82$ m s^{-2}. We evaluate the displacement field along two surface profiles (1 and 2) each of which bisect the rectangle (Fig. 2a). The horizontal components of displacement, u and v, for profile 1 are depicted by the pair of curves in Fig. 2(b), and the equivalent results for profile 2 are shown in Fig. 2(c). The vertical component of displacement, w, for profiles 1 and 2 are also depicted using continuous curves in Figs 2(d) and (e), respectively.

For this idealized lake load, we compare the analytic results (43)–(45) with the well-known formulae for the elastic displacements associated with circular or disc loads (Farrell 1972) as follows. We approximate the rectangle with a set of 800 abutting but non-overlapping circles, each with a radius of 25 m, organized into a 20 × 40 grid (the grey circles in Fig. 2a). The pressure in each of these circles is set to $\frac{A_r}{A_c}p$ where p is the pressure applied within the rectangle, A_r is the area of the rectangle, and A_c is the combined area of all 800 circles used to approximate the rectangular load. This ensures an equivalence in the net force associated with the rectangular load and the approximating suite of disc loads. The net displacements associated with the suite of disc loads are determined by linear superposition. These results are indicated in Figs 2(b) and (c) by the small circular symbols. Note the excellent agreement between the numerical approximation based on disc loads and the exact result (43)–(45) obtained for the rectangular load.

4.2 Simulating a point load: subsurface displacements

Since our first test involves a comparison of displacements at points confined to the surface of the half-space, we have chosen an additional test that involves computing displacements in the interior of the half-space. We use the solution to Love's problem (a rectangular load) to

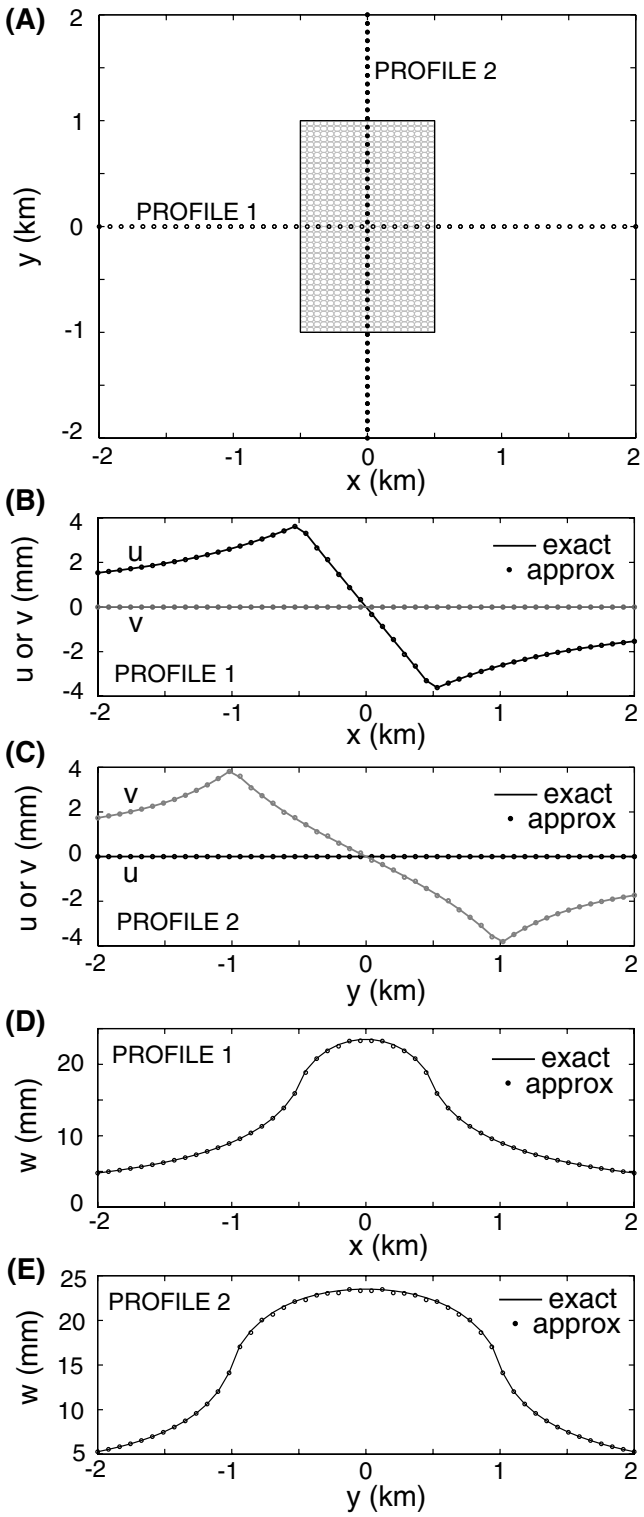

Figure 2. Displacements generated by a 2 km × 1 km rectangular load of uniform surface pressure $p = 9.82 \times 10^5$ Pa in a semi-infinite solid for which $E = 0.6 \times 10^{11}$ N m^{-2} and $\nu = 0.25$. (a) Plan-view of the rectangular load with surface profiles indicated. (b) Horizontal displacements evaluated along profile 1 using (43) and (44) (solid curve) and the numerical results for the approximating suite of disc loads (dots). (c) Same as (b) but for profile 2. (d) Vertical displacements evaluated along profile 1 using (45) (solid curve) and the numerical results for the approximating suite of disc loads (dots). (e) Same as (d) but for profile 2.

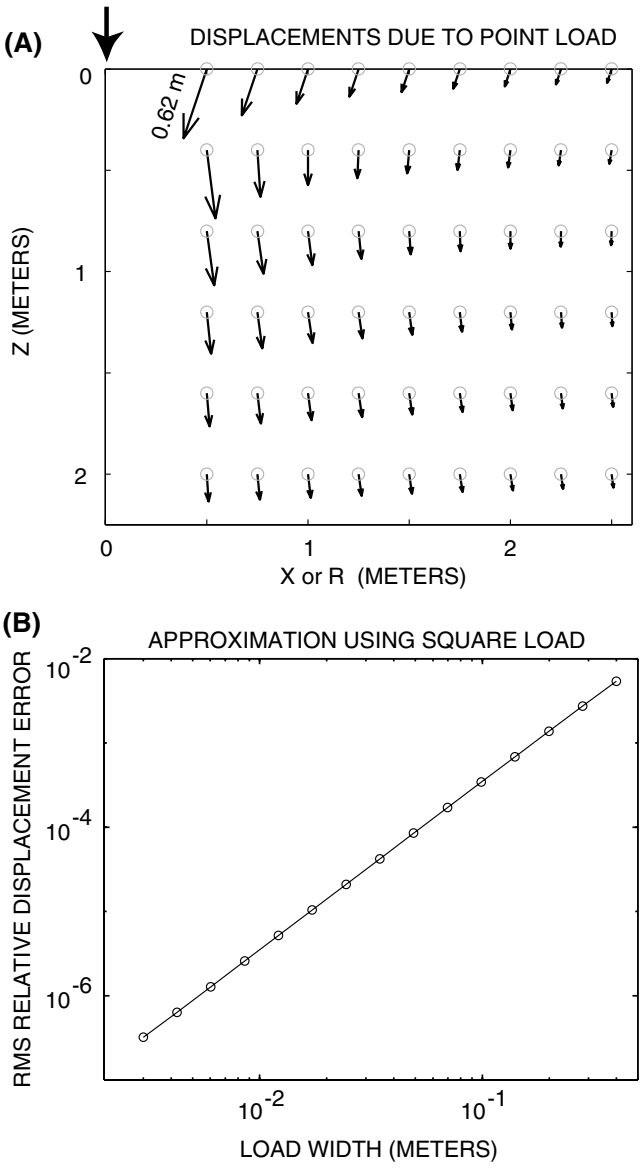

Figure 3. Comparison of the displacement field driven by a point force with the present analytical results (43)–(45) for a square region of width q for $q \to 0$. (a) Grid of the displacement field offset laterally from the point load with Boussinesq's point load solution indicated by the arrows. (b) rms relative displacement error, rms(ε), between Boussinesq's solution for a point load and Love's solution for a square load as a function of q.

approximate the solution to Boussinesq's problem, i.e. the elastic response due to a point load (Boussinesq 1885; Farrell 1972). Since the displacement field driven by a point force is singular beneath the load (i.e. the displacement there is infinite) we choose to examine the displacement field at a set of points which are offset laterally from the point load. These points, which form a 9 by 6 grid in a vertical plane, are depicted by the circles in Fig. 3(a). The displacement field driven by a point load is radially symmetric and is computed in cylindrical coordinates. We set $E = 1$ N m^{-2} and $\nu = 0.25$, and compute the displacement field associated with a unit downward force located at the origin of the coordinate system. This displacement field is depicted in Fig. 3(a). The largest displacement, 0.629 m, occurs at the gridpoint closest to the point load. We shall refer to the displacement vector computed at any gridpoint as $\mathbf{d}_{\mathrm{B}}$, where the subscript B indicates that this is the solution to the Boussinesq problem.

Next we solve the problem of the displacement field associated with a uniform pressure p applied within a square of width q, where $p = \frac{1}{q^2}$, so that the net force has unit value. The square is centred at the origin of the (now rectangular) coordinate system. As q is reduced relative to the distance between the centre of the load and the nearest gridpoint, the displacement field evaluated at our grid of stations should approach that associated with the unit point load. Let the displacement vector at any gridpoint due to the square load be $\mathbf{d}_{\mathrm{L}}$, where the subscript L indicates that this is the solution to Love's problem. Since we are attempting to approximate the solution to the point load problem we define the relative displacement error, ε, at any gridpoint to be $\frac{\|\mathbf{d}_{\mathrm{L}} - \mathbf{d}_{\mathrm{B}}\|}{\|\mathbf{d}_{\mathrm{B}}\|}$, where $\|\mathbf{d}\|$ indicates the Euclidean length of vector $\mathbf{d}$. To evaluate the approximation error, we compute the rms value of ε over the 9 by 6 grid of stations, for each value of q. We have computed this statistic for a range of square load widths between 3 mm and 0.4 m, and present the results in Fig. 3(b). Note that this is a log–log plot, and that the

best-fitting line has a slope that is very close to 2; it is seen that if the square load has a width that is very small compared with the distance to the nearest station (where we compute displacement) then the solution is very similar to that associated with a point load. We have repeated this experiment keeping $E = 1$ but allowing ν to take a range of values between 0 and 0.499, The directional fabric of the displacement field depicted in Fig. 3(a) changes significantly as ν varies, but the error plot presented in Fig. 3(b) is completely insensitive to the value of ν.

4.3 Some numerical considerations

We note that care must be taken when evaluating (43)–(45) numerically for surface displacements ($z = 0$) and for $x = \pm a$ and $y = \pm b$. Two sources of numerical difficulties arise: (1) logarithms the where the arguments go to zero for $x = \pm a$ and/or $y = \pm b$ and (2) arctangents where the arguments must be replaced by a limiting form as described below.

In case (1), all singular logarithms are multiplied by algebraic factors that go to zero; hence, the expressions for the displacements (43)–(45) are regular. For example, the last term on the right-hand side of (43) becomes infinite at the corners of the rectangle since its argument goes to zero when $z = 0$. It is straightforward to show, however, that

$$\lim_{z\to 0}\left[\frac{z}{\mu}\log(\Delta y + r_{j0})\right]_{y'=b} = 0, \qquad x = \pm a \qquad y = b (j = 1, 2)$$

and

$$\lim_{z\to 0}\left[\frac{z}{\mu}\log(\Delta y + r_{j0})\right]_{y'=-b} = 0, \qquad x = \pm a \qquad y = -b (j = 1, 2)$$

and the horizontal surface displacement is finite. These terms are explicitly set to their analytic limit of zero in the numerical code. Similar terms involving logarithms with vanishing arguments occur in (44) and in the evaluation of J_j, K_j, L_j and M_j ($j = 1, 2$). All are multiplied by algebraic factors that tend to zero more rapidly than the logarithm becomes singular; hence, these terms are explicitly set to zero in the numerical scheme.

In case (2), numerical difficulties in the horizontal displacements are avoided by simplifying the argument of the arctangent terms in J_j (14) and K_j (23) for $z = 0$. For example in (14), we replace

$$\tan^{-1}\left(\frac{|a \mp x|\psi_{j0}}{z + \beta_{j0}}\bigg|_{z=0}\right) = \tan^{-1}\left[\frac{|a \mp x|\psi_{j0}}{\sqrt{(a \mp x)^2}}\right] = \tan^{-1}\psi_{j0} \quad (j = 1, 2)$$

with similar modification for the arctangent terms in (23). For subsurface vertical displacements ($w|_{z\neq 0}$), the arguments of the arctangents are simplified as described above when $x = \pm a$ in L_j, (39) and when $y = \pm b$ in M_j, (42). When $z = 0$, the expressions for vertical displacements (45) simplify considerably to

$$w|_{z=0} = \frac{p}{4\pi\mu}\left[\frac{\lambda + 2\mu}{\lambda + \mu}(L_1 - L_2)_{z=0}\right]_{y'=-b}^{y'=b} = \frac{p}{4\pi\mu}\left[\frac{\lambda + 2\mu}{\lambda + \mu}(M_1 - M_2)_{z=0}\right]_{x'=-a}^{x'=a}. \tag{46}$$

A copy of the MATLAB® code* for the displacements (43)–(45) may be obtained from the authors upon request.

REFERENCES

Boussinesq, J., 1885. *Application des Potentiels à l'Étude de l'Équilibre et du Mouvement des Solides Élastiques,* p. 508 Gauthier-Villars, Paris.

Dong, D., Fang, P., Bock, Y., Cheng, M. & Miyazaki, S., 2002. Anatomy of apparent seasonal variations from GPS-derived site position time series, *J. geophys. Res.,* **107,** ETG, 9.1–9.18.

Elósegui, P., Davis, J.L., Mitrovica, J.X., Bennett, R.A. & Wernicke, B.P., 2003. Crustal loading near Great Salt Lake, Utah, *Geophys. Res. Lett.,* **30,** 1111–1114.

Farrell, W.E., 1972. Deformation of the earth by surface loads, *Rev. Geophys. Space Phys.,* **10,** 761–797.

Heki, K., 2001. Seasonal modulation of interseismic strain buildup in Northeastern Japan driven by snow loads, *Science,* **293,** 89–92.

Lamb, H., 1902. On Boussinesq's problem, *Proc. London Math. Soc.,* **34,** 276–284.

Love, A.E.H., 1929. The stress produced in a semi-infinite solid by pressure on part of the boundary, *Phil. Trans. R. Soc. Lond.* A, **667,** 377–420.

Mangiarotti, S., Cazenave, A., Soudarin, L. & Cretaux, J., 2001. Annual vertical crustal motions predicted from surface mass redistribution and observed by space geodesy, *J. geophys. Res.,* **106,** 4277–4291.

Terazawa, K., 1916. On the elastic equilibrium of a semi-infinite solid, *Tokyo J. Coll. Sci.,* **37,** Art. 7.

*MATLAB is a registered trademark of The MathWorks, Inc., Natick, MA, USA. http://www.mathworks.com/